ACS OMEGA

Open Access

http://pubs.acs.org/journal/acsodf

Article

Preparation and Characterization of Novel Hydroxyapatite/Montmorillonite/Gelatin-Based Composites with Bone Remineralizing Potential

José M. Posada-Lotero, Maby M. Martínez-Garzón,* Milton Rosero-Moreano, Francy N. Jiménez-García, Laura R. Giraldo-Torres, and Daniel F. Hincapié-Rojas

Cite This: *ACS Omega* 2025, 10, 15116−15128

Read Online

ACCESS | Metrics & More | Article Recommendations

ABSTRACT: Bone wear caused by injury or deterioration due to age leads to the use of autologous and allogeneic implants that are sometimes rejected by the body. Currently, work is being carried out on the development of composites that induce bone repair. In this study, composites with montmorillonite clay (MMT), hydroxyapatite (HAp), and gelatin were prepared. Initially, various ratios of HAp/MMT composites (1:1, 2:1, and 1:2) were examined, and the 2:1 ratio provided a better biological response. Finally, the HAp/MMT/Gel ternary mixtures were prepared using different percentages of gelatin: 10, 50, and 90% and maintaining the 2:1 HAp/MMT ratio. All materials were assayed in a biomineralization proof using simulated biological fluids. In the HAp/MMT/Gel diffraction pattern, the peaks associated with MMT and HAp are preserved at 20 and 32° in 2θ, respectively; the addition of gelatin promotes structural changes. Biocompatibility studies show that there are no morphological changes in the platelets since it does not exceed 5 μm of pseudopodia, which suggests that there is no rejection of the material. On the other hand, the biomineralization study, followed by SEM and FTIR characterization, showed the generation of apatite and demonstrated its potential application in bone tissue regeneration.

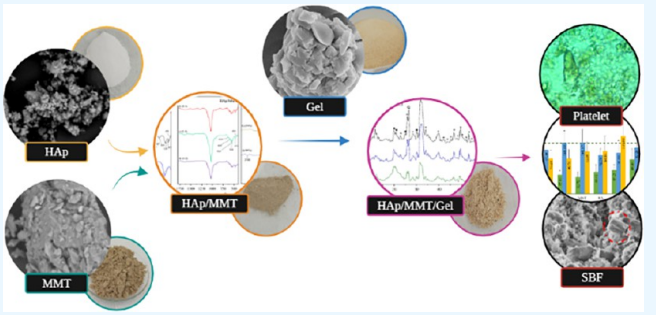

1. INTRODUCTION

In recent years, injuries and wear in bone tissues have usually been treated surgically through autologous and allogeneic implants, which sometimes involve rejection of the organism. The cellular matrix of bone tissues contains organic and inorganic materials that interact with the implant material through components such as glycosaminoglycans, collagen types I and III, and hydroxyapatite.[1] This has led the scientific community to focus its research on materials with potential applications in bone regeneration that could play a fundamental role in the development of new therapies.[1] Current approaches have focused on the design of composite materials of synthetic or natural origin that are biocompatible or bioactive.[2] One natural polymer that has been explored for the fabrication of these materials is gelatin ($NH_2COOH-CH-R$). This protein is obtained by the hydrolytic process of collagen and contains the amino acids: glycine, aspartic acid, and arginine, which favor cell adhesion and proliferation; additionally, it is biocompatible, noncytotoxic, and biodegradable.[3]

Another material used in the manufacture of these materials is hydroxyapatite (HAp: $Ca_{10}(PO_4)_6(OH)_2$), a bioactive ceramic characterized by its osteoconductive, nontoxic, and biocompatible capacity, which promotes cell proliferation and osteoblastic cell differentiation, due to its bioactivity.[4] HAp can bond with natural bone to promote an interaction between the host bone and inserted material.[5,6] However, materials based on this bioceramic have high porosity and brittleness, which affects their mechanical properties and limits their use in tissue regeneration.[5,7−9] One material used to overcome the limitations of HAp is the biocompatible clay montmorillonite (MMT: $(Na, Ca)_{0.3}(Al, Mg)_2Si_4O_{10}(OH)_2{-}nH_2O$), which is a member of the smectite group of clays.[10,11] The MMT is composed of two tetrahedral silica sheets sandwiched between a central octahedral alumina sheet. Its adsorptive capacity, high surface area, and filling capacity allow the interaction with various compounds, which improves the mechanical and thermal properties of the developed material.[12−15]

Received: November 25, 2024
Revised: February 23, 2025
Accepted: March 21, 2025
Published: April 13, 2025

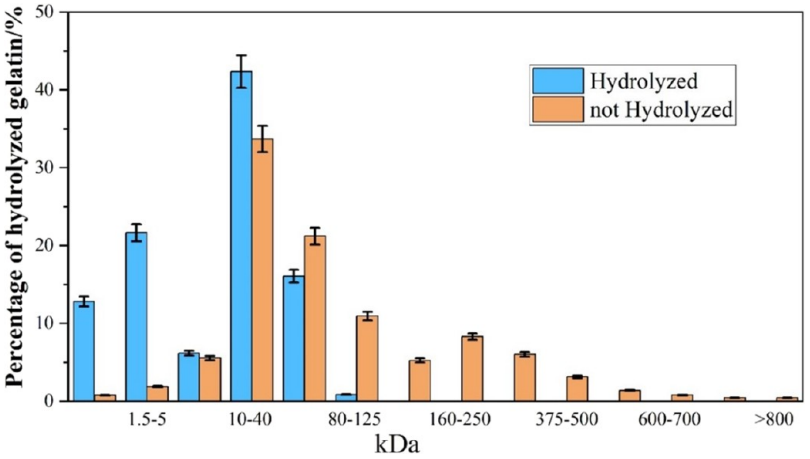

Figure 1. Molecular weight distribution of gelatin by HP SEC-UV.

In the literature, there are reports of Gel/HAp,[16] Gel/nHAp,[17] Gel/MMT,[15,18,19] and HAp/MMT,[20] in which improvements in mechanical strength, bioactivity, cell adhesion, thermal resistance, among others, are reported.[21] These characteristics mean that the synthesized material has potential application in tissue engineering.[22,23] However, the reports found on the preparation of materials from the mixture of HAp, MMT, and Gel in one pot are limited.[24] In the present work, novel composites were prepared from HAp, MMT, and Gel; first HAp/MMT binary mixture in weight ratios 1:2, 1:1, and 2:1 and, subsequently, HAp/MMT/Gel ternary mixture in mass ratios 10, 50, and 90% of gelatin starting from the HAp/MMT 2:1 binary mixture. The characterization of these compounds involves X-ray diffraction (XRD), scanning electron microscopy (SEM), Fourier transform infrared spectroscopy (FTIR), thermogravimetric analysis (TGA), nitrogen adsorption and desorption isotherms (BET), and Z-potential. The biocompatibility study of the compounds was carried out using human plasma and simulated biological fluid (SBF).

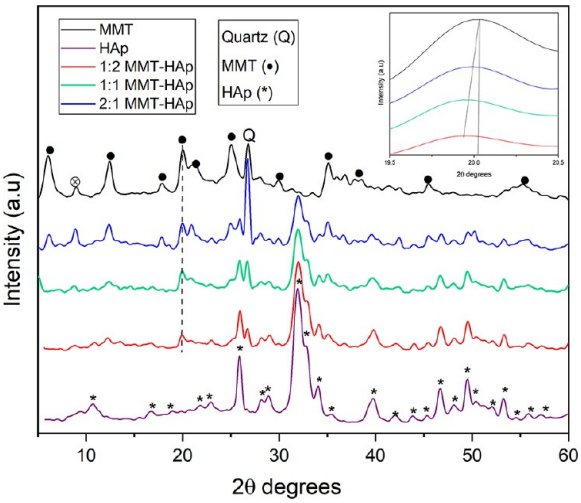

Figure 2. XRD patterns of samples HAp, MMT, HAp/MMT 2:1, HAp/MMT 1:1, and HAp/MMT 1:2. Inset: shift at peak $2\theta = 20.08°$ in the XRD patterns of the binary mixtures.

2. RESULTS AND DISCUSSION

2.1. Distribution of Molecular Weights by HPLC-SEC. The molecular weight distribution of hydrolyzed and unhydrolyzed gelatin was determined by high-performance liquid chromatography-size exclusion (HPLC-SEC) in a molecular exclusion column; the values obtained are presented in Figure 1. The unhydrolyzed sample presents a size distribution between 1.5 and 800 kDa, while the hydrolyzed sample presents a size distribution between 1.5 and 80 kDa. This size reduction is because the hydrolysis process generates the breaking of protein bonds by the endopeptidase enzyme. The use of hydrolyzed gelatin provides proteins of lower molecular mass and greater availability of −COO− and $-NH_3^+$ groups to interact with precursor materials and the extracellular environment. The gelatin is known for its ability to absorb water. This characteristic is highly valued in tissue regeneration since porosity ensures the diffusion of nutrients as well as oxygen for proper cell growth.[25]

2.2. X-ray Diffraction Analysis. Figure 2 presents the X-ray diffraction patterns of both the precursors and binary mixtures (where Quartzo:Q, MMT:• y HAp:*). In the XRD pattern of MMT, characteristic diffraction peaks of this clay are observed at 2θ = 5.88, 12.28, 17.80, 20.08, 20.95, 25.30, and 35.26°, besides other phases such as muscovite at $2\theta = 8.95°$ and quartz at $2\theta = 26.71°$ are presented. In the HAp diffractogram, the characteristic peaks of this material, according to the ICCD-JCDPS chart (09-0432), are observed. Peaks of higher intensity are observed at 2θ = 25.8, 31.72, and 32.94°; $2\theta = 34.12°$

In the binary mixture, it is observed that for the HAp/MMT 2:1, the intensity of the peaks associated with MMT begins to decrease and those associated with HAp increase, which is evidence that a mixture of precursors has been obtained. For the samples HAp/MMT 1:1 and HAp/MMT 1:2, the MMT peaks at low angles almost disappear, and those associated with HAp continue to grow in intensity. The inset in Figure 2 shows how, as the amount of HAp in the mixtures increases, there are shifts in the peak at $2\theta = 20.08°$ assigned to MMT and present in the three samples. The values of the shift and peak widths are presented in Table 1. This shift of the peak toward lower angles may be associated with a broadening in the interlaminar space of the MMT due to the exchange of Ca^{2+} ions from HAp with other ions of the MMT by isomorphic substitutions.[26,27] In addition, the peak broadening is observed to decrease, which is indicative of a larger particle size.

https://doi.org/10.1021/acsomega.4c10725
ACS Omega 2025, 10, 15116−15128

Table 1. Shift at Peak 2θ = 20.08° in the X-ray Diffraction Patterns of Binary Mixture

sample	2θ (degrees)	w (degrees)	shifting (degrees)
MMT	20.0004	0.8179	
HAp/MMT 1:2	19.989	0.7644	0.015
HAp/MMT 1:1	19.959	0.5905	0.045
HAp/MMT 2:1	19.935	0.5677	0.069

The HAp/MMT 2:1 binary mixture was selected to obtain the ternary mixtures since it presents a greater incorporation of calcium in the structure, good stability to pH changes, and greater surface area (which will be discussed later). Figure 3

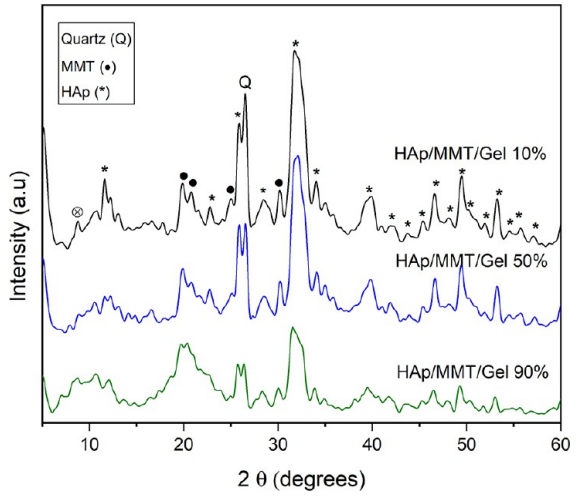

Figure 3. XRD patterns of HAp/MMT/Gel10%, HAp/MMT/Gel50%, and HAp/MMTGel90% samples.

shows the XRD patterns of the samples with gelatin: HAp/MMT/Gel10%, HAp/MMT/Gel50%, and HAp/MMT/Gel90%. Gelatin is observed to decrease crystallinity, indicating the formation of exfoliated structures.[24] This behavior could be associated with the intercalation of proteins since the higher the proportion of gelatin the sample presents a more amorphous structure. Despite the low crystallinity observed in the pattern of the material with 90% gelatin, there are broad peaks around 2θ = 20° associated with MMT, and 2θ = 32° associated with HAp, and a similar behavior to that of the 2:1 HAp/MMT binary mixture, which is the basis for the preparation of the ternary mixtures.

2.3. Thermogravimetric Analysis. The TGA thermograms and derivatives of the thermograms (DTGA) of the precursor materials and binary and ternary mixture are shown in Figure 4.

Figure 4a shows the three stages of decomposition for HAp. The first stage ranges from room temperature to 200 °C and corresponds to the elimination of water absorbed in the sample (2.87% of the total mass of the material). The second stage occurs between 200 and 570 °C and corresponds to the decomposition of HPO_4^{-2} (in this stage, 2.5% of the total mass was eliminated).[28] Furthermore, in the range between 700 and 815 °C, HAp decomposes, which corresponds to 0.59% of the total mass.[28−30] Finally, at a temperature of 900 °C, a residue of 93.61% is obtained.[28−30] These results agree with those reported by Bernatal Saragih, Ika Karyati.[22] Figure 4b shows the thermal decomposition of MMT; in this case, three stages of decomposition are also observed. The first occurs between room temperature and 200 °C and corresponds to the elimination of physisorbed water, in addition to the removal of physisorbed species, such as N_2 or CO_2. In this case, 5.56% of the total mass of the material was eliminated. The second stage occurs in a range between 220 and 232 °C and involves the decomposition of organic species where 1.16% was eliminated. Finally, between 340 and 800 °C, dehydration and subsequent decomposition of the alunogen and dihydroxylation of the aluminosilicate layers of the montmorillonite occur, as well as the decomposition of products associated with the organic carbonaceous residue.[5] In this last stage, 6.93% of the material was eliminated. The residue obtained in this case is 86.05%. These results indicate that HAp presents greater stability than MMT due to its mostly inorganic chemical composition.

Figure 4c−e shows the thermograms of the binary mixture. Four thermal decomposition events associated with the removal of moisture from the sample, the dehydration of HAp and MMT phases, such as muscovite, and the presence of aluminosilicates in the material are evident. Additionally, it is observed that the mass removal for the third stage of decomposition of this sample, in the temperature range between 340 and 900 °C, is lower compared to that for the other composites. This is because this sample has the lowest MMT content, and in this temperature range, dehydration of the alunogen and dihydroxylation of MMT is favored.[30]

In Figure 4f−h, the thermograms of the ternary mixture are presented. In all samples, six stages of decomposition were identified in the material. The first stage corresponds to the elimination of water due to the humidity of the sample, which occurs in a range between 25 and 160 °C. As the gelatin content increases, the material's water absorption also rises due to its hydrophilic functional groups, which attract water and retain it through hydrogen bonds. The second range of decomposition occurs between 160 and 590 °C and corresponds to the decomposition of the HPO_4^{-2} of HAp, the decomposition of organic species, and the dehydration and subsequent decomposition of the alunogen of MMT. Additionally, the decomposition of gelatin occurs due to the degradation of protein bonds and the denaturation and thermal decomposition process. In the HAp/MMT/Gel 90% sample (see Figure 5h), whose gelatin content is higher, only one decomposition event can be identified because the greater mass loss of the material is associated with the decomposition of gelatin.[31,32] Above 700 °C, MMT decomposes (Figure 4f). However, with a higher gelatin content, less mass is lost from these compounds (Figure 4g,h), particularly in the 90% gelatin sample. The residues were 83.84, 55.55, and 27.07% for samples with 10, 50, and 90% gelatin, respectively, indicating that higher gelatin content leads to greater mass loss as its organic components decompose at lower temperatures than the inorganic ones in HAp and MMT.

2.4. Fourier Transform Infrared Spectroscopy. The FTIR spectra of the precursors, binary, and ternary mixtures are presented in Figure 5. Figure 5a presents the FTIR spectrum of gelatin in which bands are observed at 1077 cm^{-1} associated with the C−O−C stretching mode; 1450 cm^{-1} related to CH_2 and CH_3 vibrations; and at 1539 cm^{-1}, which correspond to symmetric and asymmetric vibrations of the amide groups of the protein. In addition, the band around 1648 cm^{-1} is attributed to vibrations of the C=O group and the band around 2930 cm^{-1} is attributed to C−H vibrations.[29,33−35] The band between 3000 and 3700 cm^{-1} is

https://doi.org/10.1021/acsomega.4c10725
ACS Omega 2025, 10, 15116−15128

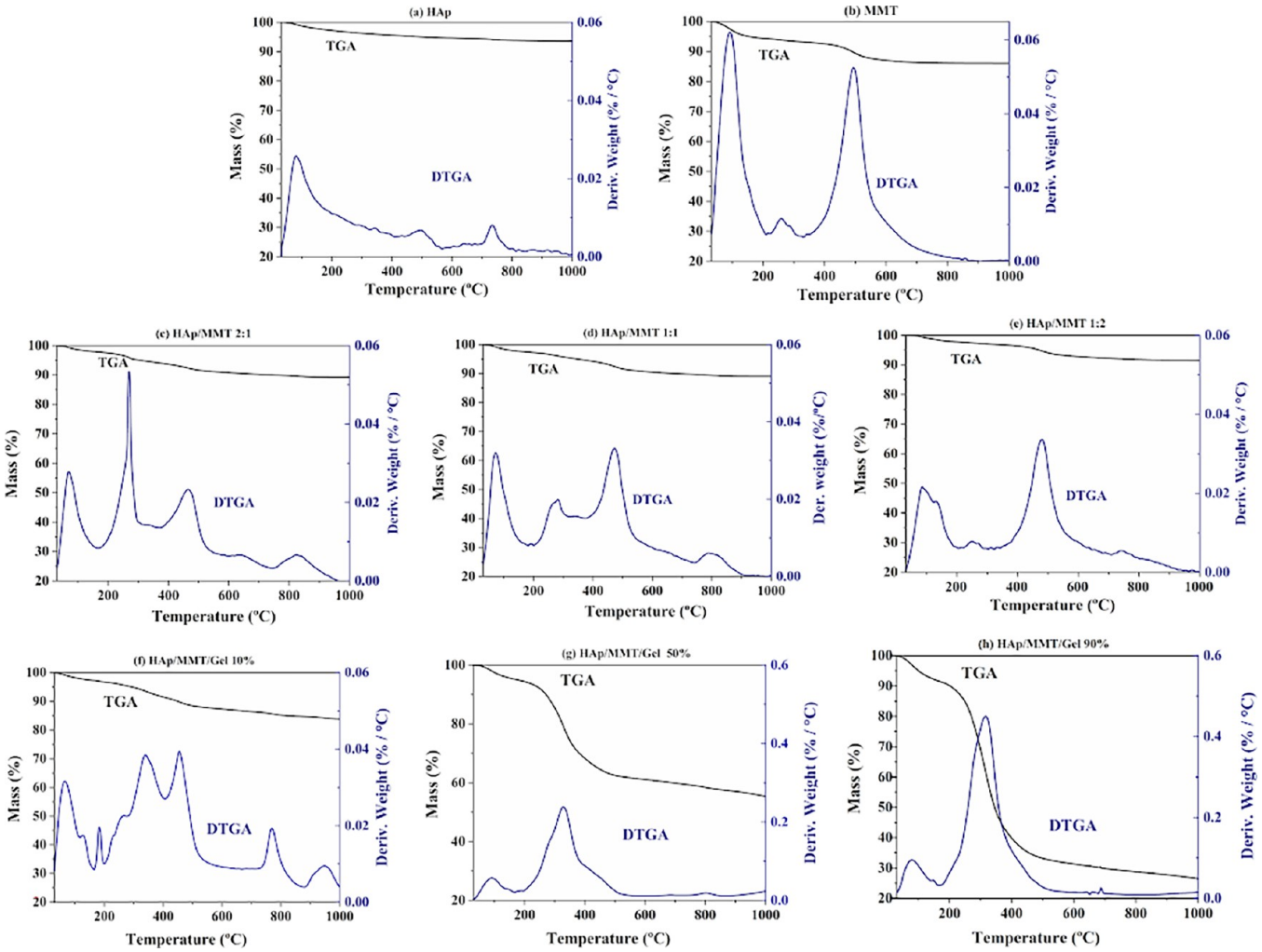

Figure 4. Thermograms TGA/DTGA of (a) HAp, (b) MMT, (c) HAp/MMT 2:1, (d) HAp/MMT 1:1, (e) HAp/MMT 1:2, (f) HAp/MMT/Gel10%, (g) HAp/MMT/Gel50%, and (h) HAp/MMT/Gel90%.

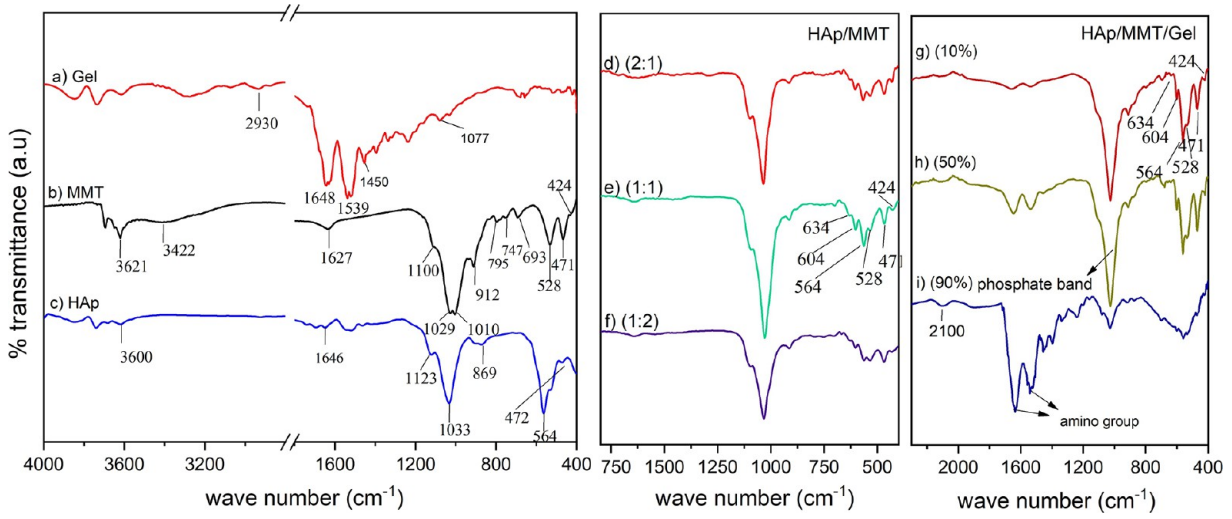

Figure 5. FTIR spectra of the materials (a) Gel, (b) MMT, (c) HAp, (d) 2:1 HAp/MMT, (e) 1:1 HAp/MMT, (f) 1:2 HAp/MMT, (g) HAp/MMT/Gel10%, (h) HAp/MMT/Gel 50%, and (i) HAp/MMT/Gel 90%.

related to the presence of water in the material, which is consistent with the hydrophilic characteristics of gelatin.

In Figure 5b, the vibrational modes for MMT have been identified. A band is observed at 424 cm^{-1} associated with bending vibrational modes for the Si−O−Si or Al−OH of muscovite, a phase that was identified in XRD. Other bands are evident at 471 cm^{-1} associated with Si−O−Si deformation, at 528 cm^{-1} attributed to Si−O−Al deformation,[29] and at 693

https://doi.org/10.1021/acsomega.4c10725
ACS Omega 2025, 10, 15116−15128

and 912 cm^{-1} assigned to Al−Al−OH bending.[30] At 747 and 795 cm^{-1} bands associated with quartz are observed, which was identified by XRD. Around 1000 cm^{-1}, an intense band appears, which is assigned to Si−O vibrations of the Si−O−Si group of mineral clays.[28,33] The band at 1627 cm^{-1} is attributed to the −OH deformation of water,[28] another at 3422 cm^{-1} to the OH stretching of water,[28] and one at 3621 cm^{-1} to the −OH stretching mode of water at the inner surface of the MMT.[36]

Figure 5c shows the spectrum of HAp. The vibrational modes of the phosphate groups PO_4^{-3} at 472 cm^{-1}, v2, 564 cm^{-1}, v4, and around 1033 cm^{-1}, and v3 are identified. The band at 869 cm^{-1} is associated with vibrational modes of the HPO_4-v5 groups; in addition, a vibrational mode is evident around 1653 cm^{-1} assigned to the OH groups of HAp.[37] The band at 3600 cm^{-1} is assigned to vibrations of adsorbed water on the material.[37] Figure 5d−f shows the FTIR spectra of the HAp/MMT binary mixture in their different ratios. The presence of functional groups characteristic of MMT (471 and 528 cm^{-1}), muscovite (424 cm^{-1}), and HAp (564 cm^{-1}) is evidenced between 400 and 600 cm^{-1}, as previously discussed. In addition, in all the binary mixtures, vibrational modes become more evident at 604 cm^{-1}, associated with v4 vibrations of the phosphate group, and at 634 cm^{-1} to OH groups in the HAp.[35]

Figure 5g−i shows the FTIR spectra of the ternary mixtures, in which the presence of the characteristic vibrations of MMT, HAp, and gelatin is evident. In these spectra, broad absorption bands are observed between 3000 to 3700 cm^{-1} due to physisorbed water, in which the bands assigned to the OH groups of HAp and MMT overlap.[38,39] The broad band at 1030 cm^{-1}, which overlaps the vibration of PO_3^{-2} in HAp with the extension of the Si−O−Si mode of MMT, appears in all of the samples; however, its intensity is significantly reduced in the material containing 90% gelatin due to the low concentration of MMT and HAp. In all materials, bands are observed around 1648, 1539, and 1450 cm^{-1} corresponding to characteristic vibrations of gelatin functional groups,[40] but with higher intensity, as expected, in the sample containing 90% gelatin. A band is observed at 2100 cm^{-1} cm whose presence can be attributed to the interaction of the C−N groups of gelatin with the OH groups of HAp or MMT, which is more intense for the sample with 90% gelatin.[33,41]

2.5. Specific Surface Area and Porosity. Figure 6 shows the nitrogen adsorption−desorption isotherms for HAp, MMT, HAp/MMT 1:1, and HAp/MMT/Gel 50%. These isotherms correspond to type III, which is related to materials with extended porosity or macroporous and indicates a low adsorbate−adsorbent interaction. This type of isotherm suggests the formation of multiple adsorbate layers on the surface of the material. All materials exhibit adsorption below 50 cm^3/g for P/Po values <0.8, indicating weak adsorbate−adsorbate interaction. When P/Po exceeds the value of 0.8, the amount of adsorbed gas increases rapidly, i.e., adsorbate−adsorbent interactions are strongest in this region. The amount of gas absorbed in the ternary mixtures is reduced from 95 cme

The surface areas and pore volumes of the precursors and binary and ternary mixtures were measured and are presented in Table 2. For the binary mixtures, the surface area and total pore volume increase in the samples with more HAp. the surface areas of the HAp/MMT (2:1 and 1:1) are similar, with a slightly higher value for the HAp/MMT 2:1. The lowest value is for the HAp/MMT 1:2 and may be related to the low

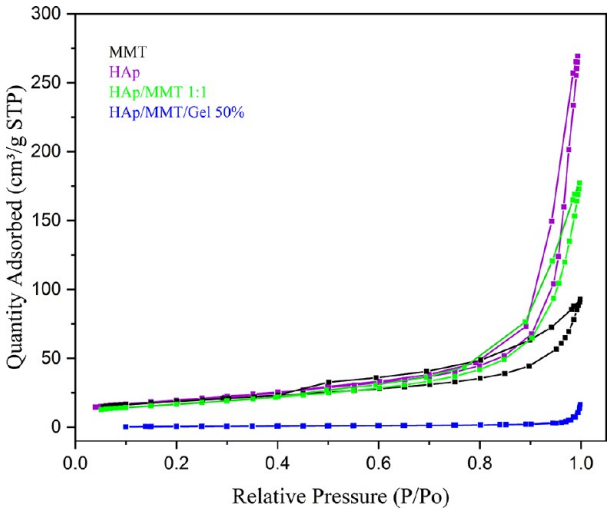

Figure 6. Nitrogen adsorption−desorption isotherms for HAp, MMT, 1:1 HAp/MMT, and HAp/MMT/Gel50%.

Table 2. BET Surface Areas and Pore Volume of HAp, MMT, HAp/MMT 2:1, HAp/MMT 1:1, HAp/MMT 1:2, HAp/MMT/Gel10%, HAp/MMT/Gel50%, and HAp/MMT/Gel90%

material	surface area BET (m^2/g)	total pore volume (cm^3/g)
HAp	70.0012	0.416716
MMT	67.1447	0.143630
HAp/MMT 1:2	49.8723	0.181205
HAp/MMT 1:1	60.0685	0.273826
HAp/MMT 2:1	60.4725	0.366077
HAp/MMT/Gel10%	17.9675	0.146485
HAp/MMT/Gel50%	2.6453	0.025393
HAp/MMT/Gel90%	0.0067	0.001328

pore volume of the MMT as these pores are predominant in the sample due to a higher amount of MMT used. Concerning the ternary mixtures, it is evident that the pore volume and surface area decrease with increasing gelatin content. This decrease may be due to the pores being filled with gelatin proteins, which after the hydrolysis process reach smaller particle sizes.

2.6. Z-Potential Analysis. The Z-potential is a measure of the electrical charges of a suspension that allows the identification of solid−liquid interface conditions, surface interactions, and suspension stability, especially for colloids or nanometric materials.[42,43] This potential provides information about the stability of a material to changes in pH and ionic strength.[44] A value close to ± 30 mV or higher indicates that the compound is more stable, i.e., there is a balance between the electrical repulsions of the surface charge and the attractive van der Waals forces.[44] Table 3 shows the values for the different samples in this study. As can be evidenced, HAp is a material sensitive to changes in pH and ionic strength (−1.8 mV), while MMT is more stable to these changes (−20.5 mV). In this sense, the interaction between HAp and MMT provides a more stable material compared to the precursor materials. The HAp/MMT 2:1 and 1:1 binary mixture presents the highest Z-potential values, which may allow the possible interactions of the material with the extracellular environment and improve its bioactivity and biocompatibility. In turn, the gelatin shows a positive potential of 5.07 mV related to

https://doi.org/10.1021/acsomega.4c10725
ACS Omega 2025, 10, 15116−15128

Table 3. Potential Values for MMT, HAp, Gelatin, and the Composites Obtained

material	Z-potential (mV)
MMT	−20.5
HAp	−1.8
Gel	5.07
HAp/MMT 2:1	−35.24
HAp/MMT 1:1	−38.6
HAp/MMT 1:2	−23.7
HAp/MMT/Gel10%	−13.44
HAp/MMT/Gel50%	−15.93
HAp/MMT/Gel90%	−17.13

polymeric materials, and the values of the ternary mixtures are less than ± 30 mV, which presupposes that the presence of gelatin destabilizes the system.[44] The hydrophilic characteristics of gelatin promote its dissolution in an aqueous medium, and in addition, being an organic material, it is more sensitive to pH changes compared to inorganic materials such as HAp and MMT.

2.7. Scanning Electron Microscopy (SEM) Analysis. The morphologies of the precursors, binary, and ternary mixtures were evaluated by SEM and are presented in Figure 7, and the composition was determined by EDS (these results are not shown only discussed). HAp presents a nanometer particle morphology with submicrometric-sized agglomerates (Figure 7a) composed of Ca, P, C, and O. MMT presents a flake-like morphology between 1 and 2 μm in size that overlaps each other (Figure 7b), composed mainly of Mg, Al, Si, K, C, and O. These morphologies coincide with those reported in the literature.[10,45] In Figure 7c, the morphology of gelatin is observed, in which agglomerates of thick nonporous sheet structures of sizes around 4 μm are evidenced. SEM images of the HAp/MMT 1:1, HAp/MMT 2:1, and HA/MMT 1:2 binary mixtures are shown in Figure 7d–f, respectively. HAp over MMT is observed, which is consistent with that reported by Laabd et al.[46] As the amount of HAp in the binary mixtures

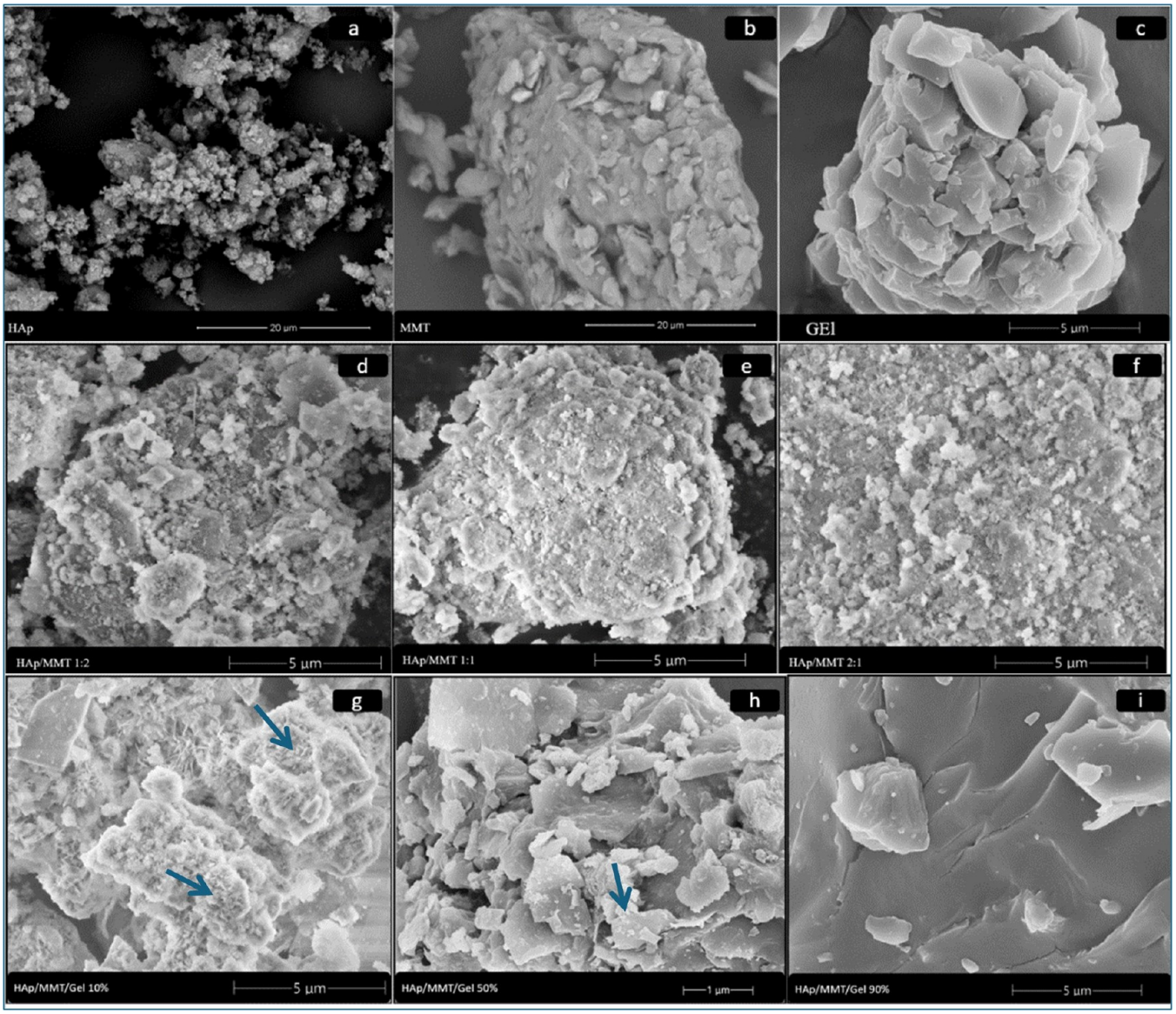

Figure 7. SEM of the materials (a) HAp, (b) MMT, (c) Gel, (d) HAp/MMT 2:1, (e) HAp/MMT 1:1, (f) HAp/MMT 1:2 (g) HAp/MMT/Gel10%, (h) HAp/MMT/Gel50%, and (i) HAp/MMT/Gel90%.

https://doi.org/10.1021/acsomega.4c10725
ACS Omega 2025, 10, 15116−15128

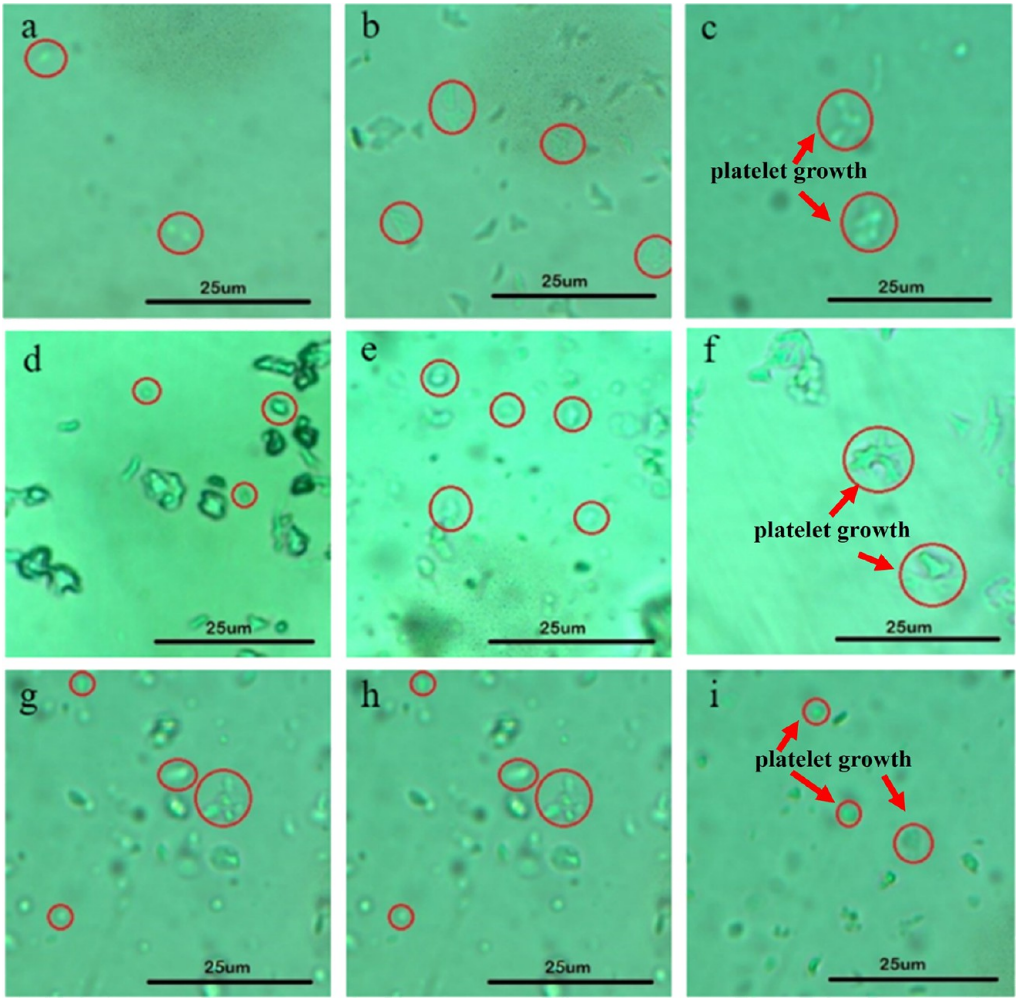

Figure 8. Platelet growth distribution: control sample min (a) 0, (b) 30, and (c) 60; HAp/MMT 1:1 min (d) 0, (e) 30, and (f) 60; and HAp/MMT/Gel90% min (g) 0, (h) 30, and (i) 60.

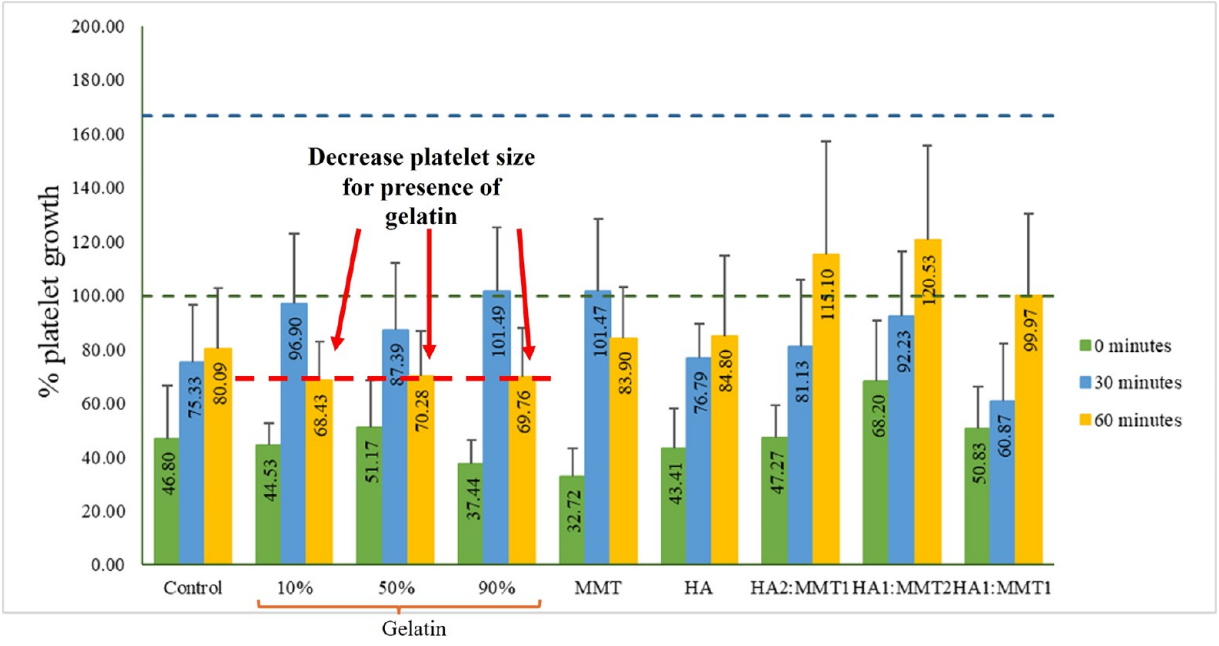

Figure 9. Biocompatibility test results.

https://doi.org/10.1021/acsomega.4c10725
ACS Omega 2025, 10, 15116−15128

increases, the MMT flakes are not as clearly observed due to a higher amount of HAp grains over the surface. In the HAp/MMT/Gel10% ternary mixture, shown in Figure 7g, the morphology is of blocks of different sizes, and porosity is evident, which agrees with the values obtained by BET for this sample. As expected, for the sample HAp/MMT/Gel50%, large agglomerates are more visible, and less porosity is evident. For HAp/MMT/Gel90%, the surface is smoother due to the predominance of gelatin (Figure 7i), which agrees with the low pore volume value obtained by BET measurements.

The atomic percentages of each element obtained by energy-dispersive X-ray Spectroscopy (EDS) for the samples with 10 and 50% gelatin, calculated as the mean of five points per sample, are presented as follows.

For the HAp/MMT/Gel10% sample: C (40.68%), O (43.37%), Al (3.19%), Si (4.83%), P (2.54%), and Ca (4.67%) and trace amounts of Fe and Na.

For the HAp/MMT/Gel50% sample: C (62.92%), O (24.20%), Al (5.01%), Si (3.81%), P (1.24%), and Ca (2.40%) and trace amounts of Fe and Mg.

The HAp/MMT/Gel50% composite exhibits a higher carbon concentration (at all analyzed points) compared to that of HAp/MMT/Gel10%, as expected due to the increased gelatin content. Notably, the region with the highest percentages of Ca and P (associated with HAp) corresponds to areas where smaller particles were detected, specifically those highlighted in blue in Figure 7g,h.

2.8. Biological Tests. A platelet count study was performed and is presented in Figures 8 and 9. It is observed that all the composites have a stable platelet behavior with a mean size of less than 5 μm[33] demonstrating that there is no platelet adhesion and suggesting that all these composites are biocompatible. Figure 8 shows micrographs of platelet growth (highlighted with red circles) for the control sample (8a, 8b, and 8c), HAp/MMT (8d, 8e, and 8f), and HAp/MMT/Gel (8g, 8h, and 8i) at 0, 30, and 60 min. For the control sample, the expected behavior of platelets according to their natural function is observed. For the binary mixtures, platelet adhesion behavior is observed with pseudopodia less than 5 μm. In all binary mixtures, the percentages of platelet size evolution increase with time; however, none exceed 5 μm. It is also observed that the percentage of platelet evolution in the gelatin-containing composites is lower than the binary mixtures at 60 min. This result may be due to the interaction of gelatin with platelet membrane glycoproteins (GP) (GP Ia-IIa, GP IV, GP VI, and GP V),[47] which helps to promote platelet integrity over time. This behavior indicates that both binary and ternary mixtures have properties that make them suitable for applications in bone regeneration, with favorability for ternary mixtures. Several studies have shown that the ideal surface of a biocompatible material should have oxygen groups, as this reduces the number of bound platelets.[47] Gelatin contains various oxygen groups both in the peptide bond and in some of the R-chains. This confirms the results obtained with the gelatin-containing material (Figure 8).

Figure 9 shows in percentage the evolution of platelet size for all the compounds whose behavior is illustrated in Figure 8. The dotted lines indicate the limits of platelet size in the blood (3 μm equals 100%) and the beginning of platelet adhesion with pseudopodia (5 μm equals 166.67%). In the ternary mixtures (10, 50, and 90%), a similar initial growth is evident to that of the binary mixture. However, after 60 min, a decrease in size is observed amounting to 28.37, 17.11, and 31.73%, respectively. It should be noted that, in Figures 8 and 9 (as indicated by the arrows), a trend is observed, when gelatin is present, there is a decrease in platelets after 60 min, which leads to the assumption that gelatin decreases platelet growth and consequently the ternary composites are more biocompatible than the other analyzed materials.

An ANOVA was performed at a significance level of $\alpha = 0.05$ to determine if there are significant differences in platelet diameter as a function of the two factors in the experiment: sample type and interaction time of the material with the platelets. The p-values obtained from the ANOVA, presented in Table 4, indicate statistically significant differences in interaction time ($p < 0.05$). In contrast, no significant differences were observed regarding sample type ($p > 0.05$). This suggests that, over time, the mean platelet diameter tends to increase, which is consistent with this type of interaction. However, it is important to note that in no case does the diameter reach 5 μm, a critical value indicating the appearance of pseudopodia in platelets. Additionally, all samples were found to be biocompatible, which is a favorable outcome of this analysis.

Table 4. Values Obtained from ANOVA

fuente	DF	SC	MC	F	P
factor (Time)	2	28,997	14,498.6	26.98	0.000000002
factor (Sample)	8	5229	653.7	1.22	0.302427903
error	70	37,618	537.4		
total	80	71,845			

On the other hand, while the inclusion of gelatin results in a lower negative charge compared to the binary mixture, as observed in the Z-potential, it has also been reported to enhance elasticity, flexibility, interaction with the extracellular environment, and cell adhesion and proliferation.[1]

To verify the biomineralization capacity of the composites, in vitro tests were carried out. The materials were immersed in SBF at a temperature of 37.5 °C; after 14 days, the mineralization ability of each material was evidenced. Figure 10 compares the morphological changes as an effect of the treatment in SBF for HAp/MMT 1:2 and Hap/MMT/Gel50%. The fact that the material interacts with SBF promotes the formation of apatite crystals whose morphology is needle-shaped, these crystals are observed growing on the montmorillonite from the original hydroxyapatite. Olad et al.[1] state that apatite formation in artificial materials is induced by negatively charged functional groups, which further induce apatite through the formation of amorphous calcium phosphate.[48] The HAp acts as a nucleation site,[49] and the MMT, by its negatively charged surface, generates a synergistic effect with HAp to induce apatite formation. Once apatite nuclei are formed, they can grow spontaneously by absorbing calcium and phosphate ions from the surrounding fluid.

In this case, the fluid is SBF, which serves as the source of calcium for this process. While the gelatin content in the ternary mixture increases, its characteristic structure evidenced in Figure 7i prevails. However, after SBF, a decrease in gelatin crystals is observed due to the washing of the material after the process and its hydrophilic nature. In addition, needle-like crystals are observed on the surface of the material, confirming the growth of apatite crystals due to the bioactive characteristics of HAp.[50] The arrows indicated in the micrographs (green for the binary composite and red for the ternary

https://doi.org/10.1021/acsomega.4c10725
ACS Omega 2025, 10, 15116−15128

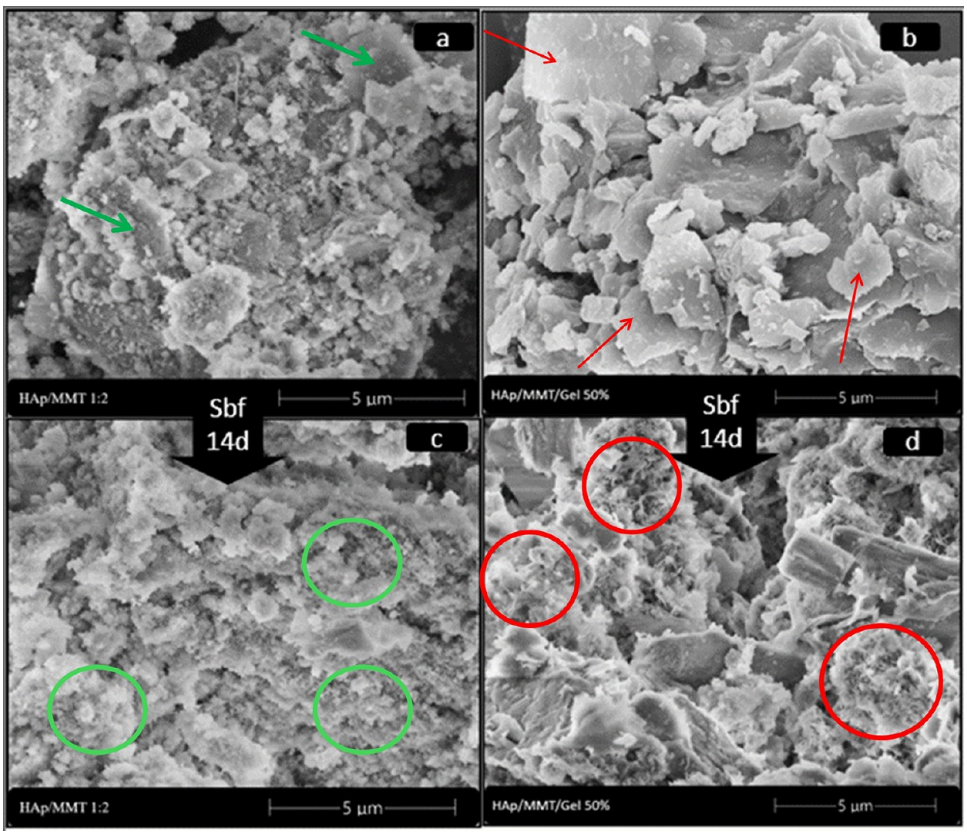

Figure 10. SEM of materials before and after SBF (a) HAp/MMT 2:1 before SBF, (b) HAp/MMT/Gel50% before SBF, (c) HAp/MMT 2:1 after SBF, and (d) HAp/MMT/Gel50% after SBF.

composite) show that before SBF immersion slightly smoother flakes are observed; the circles highlight the nucleation sites where apatite formation has occurred after SBF immersion.

FTIR analyses were also performed on the gelatin samples before the SBF test and 14 days later. Figure 11 shows the results obtained. The presence of phosphate groups is evident in the bands at 560 and 1100 cm^{-1}. These bands are present both before and after SBF, indicating that calcium phosphates are present during the interaction with the fluid, allowing them to bind to the Ca^{2+} ions present in the medium to form apatite.

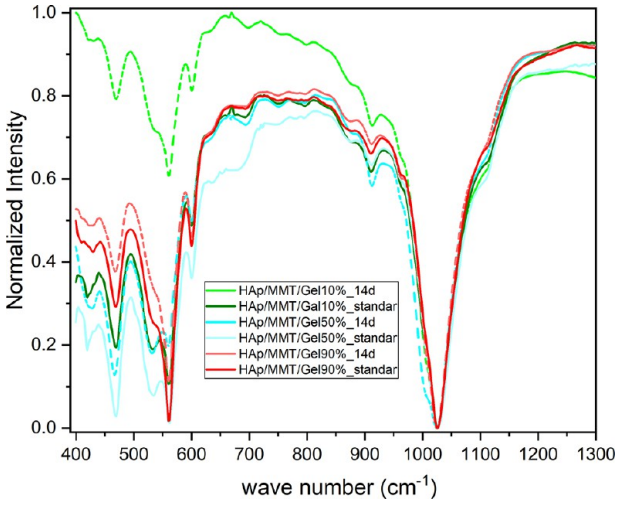

Figure 11. FTIR spectra of HAp/MMT/Gel10%, HAp/MMT/Gel90%, and HAp/MMT/Gel50% before and 14 days after SBF.

These results are consistent with the SEM images showing apatite formation after the SBF process.

Finally, for tissue regeneration to take place, it is necessary to create an optimal environment that stimulates osteoblasts to work.[51] Thus, HAp provides the necessary mineral structure for apatite formation, and gelatin, derived from collagen, facilitates cell adhesion and proliferation, all of which induce the formation of new apatite. In addition. On the other hand, negative charges stimulate apatite formation,[1] in this case, the Z potentials of the composites show that they are negatively charged, which favors the formation of new apatite. The porosity parameter directly controls the mass transfer of nutrients and metabolic waste products to the cells, as well as aiding cell migration and vascularization.[52] All these characteristics are combined and favored in the 50% gelatin composite.

3. CONCLUSIONS

In this study, HAp/MMT composites were prepared at various ratios of 1:1, 1:2, and 2:1. By TGA, the decomposition of the different phases of the precursors was evidenced, which indicates a physisorption between the components, which is ratified by the isotherms, where a low adsorbate−adsorbent interaction is evidenced. The structural changes presented in the XRD patterns indicate an ionic exchange between Ca^{2+} from HAp with ions from MMT, which evidence the interaction between both precursors. In addition, Z-potential measurements showed that the prepared binary mixtures are more stable to pH changes than their respective precursors, which is beneficial for their application in biological systems. In the platelet adhesion tests of the binary mixtures, a behavior

https://doi.org/10.1021/acsomega.4c10725
ACS Omega 2025, 10, 15116−15128

with pseudopodia of less than 5 μm was observed, which is an indication of their biocompatibility.

The 2:1 binary mixture was selected to obtain the ternary mixtures since it presents a greater surface area because of its greater amount of HAp precursor, which is characterized by supporting the bone remineralization processes. A greater number of nucleation points in the SBF test was evidenced in SEM for this sample, which allows the formation of apatite on the surface of the material.

In the comparison of the TGA results between the binary and ternary mixtures, a greater decomposition of the organic components of gelatin is evidenced in the ternary mixtures compared to the inorganic components of MMT and HAp. In the ternary mixtures, the growth of apatite crystals on the surface of the material through SBF is confirmed, which evidence its bioactive characteristics. The 50% gelatin ternary mixture presents the best response in the biocompatibility tests since it presents a similar behavior to the control sample (only platelets). In addition, this sample has more gelatin than the 10% ternary mixture, which generates an affordable environment for interaction with the cell membrane and makes it a potential tissue regenerative agent.

It is observed that the ternary mixtures are a possible alternative in tissue regeneration, since over time there is a lower percentage of platelet growth and because they have biocompatible compounds from the extracellular matrix (HAp, collagen), which allow the processes of mineralization of bone tissue in biological systems.

4. EXPERIMENTAL SECTION

The following precursors were used to obtain the binary and ternary mixtures: gelatin (humidity 11%), provided by the company S.A.S GELCO, Juanchito Industrial Park, Colombia. Montmorillonite was extracted from the Líbano-Tolima mine, a property of the company Bentominercol S.A.S., Colombia, which was purified using sodium polyphosphate ($Na_5P_3O_{10}$, 65%) and hydrochloric acid (HCl, 37%). Hydroxyapatite was synthesized by the bottom-up method from calcium nitrate ($Ca(NO_3)_2.4H_2O$, 98%), ammonium dihydrogen phosphate ($(NH_4)H_2PO_4$, 98%), and ammonia (NH_3, 100%). All of these reagents are of analytical grade (Merck Inc., Germany) and were used without further purification. Type I distilled water was used in all of the processes.

4.1. Process for Obtaining Montmorillonite. To purify the clay, 10 g of MMT, 200 mL of water, and 150 μL of 5% sodium polyphosphate (W/W) were mixed. The mixture was stirred for 90 min at 1500 rpm, and the fraction suspended for 8 h was separated by adding a 2 M hydrochloric acid solution. Subsequently, it was centrifuged at 4000 rpm for 10 min, and the paste obtained was dried at 60 °C for 48 h and sieved on a 150 μm sieve.

4.2. Process for Obtaining Hydroxyapatite. Hydroxyapatite was synthesized through the Bottom-Up method with the following precursor solutions: calcium nitrate $Ca(NO_3)_2.4H_2O$ at a concentration of 0.042 M, and ammonium dihydrogen phosphate $(NH_4)H_2PO_4$ at a concentration of 0.025 M. The precursor solutions were mixed in equal parts by slowly adding the calcium solution to the phosphate solution, with an agitation of 500 rpm and at a temperature of 37 °C ± 2 °C while adjusting the pH between 8 and 10 by adding 10% ammonia (NH_3). Subsequently, the solution was agitated for 3 h, and the pH was maintained and then allowed to stand for 48 h. After this time, it was washed with distilled water three times and filtered to remove the ammonia. Finally, it was dried at 80 °C for 12 h and the mechanical grinding process was carried out to reduce its size.[53]

4.3. Gelatin Hydrolysis Process. Gelatin was mixed with type I water to obtain a 20% W/V solution. The gelatin solution was heated to 60 °C, and NaOH was added until a pH between 7.5 and 8.0 was reached. 0.3% of the enzyme endopeptidase was added to hydrolyze the protein bonds, and the solution was stirred for 5 h at 60 °C. Subsequently, the enzyme was inactivated at 140 °C and refrigerated for 1h; finally, a light brown solid was obtained, which was reserved for subsequent preparations.

4.4. Steps for Obtaining the Composites. For the preparation of the composites, two methods were referenced: one in which HA and MMT are mixed,[26] and another that combines HA, MMT, gelatin, and chitosan through a multistep process.[1] In contrast, the proposed method simplifies the process by mixing all three precursors in a single step. This one-pot approach eliminates the need for reagents that could compromise the biomaterial properties of the composite. Although the process was initially performed in multiple stages, it was eventually streamlined into a single step as the resulting composite characteristics were found to be comparable.

Three glass flasks were used for the preparation of HAp/MMT (2:1, 1:1, and 1:2), in each of which the precursors were added according to the ratio to be used. These precursors were suspended in an aqueous solution of 1/10 of type I water, acidified with acetic acid (1% V/V), and shaken at 700 rpm for 24 h at 38 °C. They were left to stand for 1 h and filtered by washing with a 1% NaCl solution and type I water. Finally, they were dried at 35 °C and the resulting powder was macerated.

The one-pot method was used for the preparation of the ternary mixtures. Three glass flasks were used; in each one, HAp, MMT (in 2:1 ratio), and 10, 50, and 90% (concerning the total mass of the composites) of hydrolyzed gelatin were added. These mixtures were placed in a 1/10 aqueous solution (1:precursor and 10:type I water acidified with 1% acetic acid). The mixture was stirred at 700 rpm for 24 h. The obtained solid was dried at 35 °C and passed through a 150 μm sieve.

4.5. Characterization of Precursors and Composites. For the chromatographic analysis of gelatin and its molecular weight distribution, a Thermo U-Dionex HPLC instrument with an ultraviolet (UV) detector was used. An XBridgea BEH45O SEC column (3.5 mm particle size, 7.8 mm ID × 300 mm) was used at an oven temperature of 40 °C under isocratic conditions using type I water as a mobile phase at a flow rate of 1.0 mL/min. UV detection was performed at 210 nm; the analysis time was 20 min.

Structural characterization of the composites was carried out with a Malvern-Panalytical Model Empyrean 212 X-ray diffractometer (XRD), with Pixel 3D detector, Cu source (lamda = 1.541 Å) at 45 kV and 40 mA. The step was 0.05°, and the time per step was 50 s. The vibrational modes were obtained by FTIR with an OPUS TOUCH spectrophotometer. The method used was attenuated total reflectance (ATR); the resolution of the measurement was 4 cm^{-1} and in a range between 4000 and 400 cm^{-1}. Thermogravimetric analysis (TGA) and differential scanning calorimetry (DSC) were performed in a TGA/DTGA 5500 TA Instrument, from room temperature to 1000 °C with a heating ramp of 10 °/min in an air atmosphere. A Sortometro Micrometics, Model: ASAP 2020 PLUS using nitrogen as the adsorbate was used to obtain

https://doi.org/10.1021/acsomega.4c10725
ACS Omega 2025, 10, 15116−15128

the desorption absorption isotherms. The sample pretreatment was carried out at 150 °C for 500 min under high vacuum conditions for degassing. The isotherm was performed in the pressure range of 0.1−0.998 *P*/Po (30 points in adsorption and 23 points in desorption). The reported data were calculated using the BET method.

The Z-potential was determined using the Nano ZS, Zetasizer, Nano Series, and Malvern Instruments with a 4 MW He−Ne laser (k = 632.8 nm) equipped with a thermostated sample chamber. Ten mg of the sample were dissolved in 10 mL of water and then sonicated for 10 min, to improve the dispersion of the particles in the solution. All measurements were taken with a dispersion angle of 0° at room temperature. Morphological characterization was performed by SEM with a Helios 5 PFIB CXe equipment resolution: 0.6 nm at 30 kV, a Pathfinder Alpine EDS system, and an UltraDry EDS Detector.

In the biocompatibility analysis, the platelet adhesion protocol[54] was applied. Five mL of blood and 200 mg of each of the samples were used. To evaluate the biocompatibility of the composites, a camera coupled to the best scope BS-2052 biological microscope (ISO 10993-1) was used; the platelets were counted; and their average size was determined with the help of ImageJ software. The *in vitro* biomineralization test using Simulated Biological Fluid (SBF) was performed according to the protocol reported in ref 55. The temperature used in the incubator was 36.5 ± 1 °C, and monitoring was performed at 1, 3, 7, and 14 days by SEM and FTIR.

AUTHOR INFORMATION

Corresponding Author

Maby M. Martínez-Garzón − *Grupo de Investigación en Química Teórica y Bioinformática, Universidad de Caldas Facultad de Ciencias Exactas y Naturales, Manizales 170001, Colombia*; Email: maby.martinez@ucaldas.edu.co

Authors

José M. Posada-Lotero − *Grupo de Investigaciones en Cromatografía y Técnica Afines, Universidad de Caldas Facultad de Ciencias Exactas y Naturales, Manizales 170001, Colombia*

Milton Rosero-Moreano − *Grupo de Investigaciones en Cromatografía y Técnica Afines, Universidad de Caldas Facultad de Ciencias Exactas y Naturales, Manizales 170001, Colombia*

Francy N. Jiménez-García − *Grupo de Investigación en Física, Matemáticas con Énfasis en la Formación de Ingenieros, Universidad Autónoma de Manizales, Manizales 170001, Colombia; Grupo de investigación aplicaciones y enseñanza de las ciencias exactas y naturales, Universidad Nacional de Colombia Sede Manizales, Caldas 170001, Colombia;* orcid.org/0000-0003-1546-8426

Laura R. Giraldo-Torres − *Grupo de Investigación en Física, Matemáticas con Énfasis en la Formación de Ingenieros, Universidad Autónoma de Manizales, Manizales 170001, Colombia*

Daniel F. Hincapié-Rojas − *Grupo de Investigación en Física, Matemáticas con Énfasis en la Formación de Ingenieros, Universidad Autónoma de Manizales, Manizales 170001, Colombia*

Complete contact information is available at: https://pubs.acs.org/10.1021/acsomega.4c10725

Notes

The authors declare no competing financial interest.

ACKNOWLEDGMENTS

The authors thank the Universidad de Caldas, Vicerrectoría de Investigaciones y Postgrados, for the financial support of this project (code number 0311821), and the Universidad Autónoma de Manizales, Unidad de Investigación, for financing this project (code number 164-117). We also recognize the importance of the collaboration of the gelatin production company GELCO S.A.S., Juanchito Industrial Park, Colombia, for providing the gelatin for the development of this research. We also thank María Sofia Tafur Hernández, a biomedical engineering student at the Universidad Autónoma de Manizales, Manizales, for her participation in the research group.

ABBREVIATIONS

MMT:montmorillonite
HAp:hydroxyapatite
Gelatin:gelatin
BET:surface area
XRS:X-ray diffraction
FTIR:Fourier transform infrared
HPLC-SEC:high-performance liquid chromatography−size exclusion
SEM:scanning electron microscopy
TGA:thermogravimetric analysis
SBF:simulated biological serum

REFERENCES

(1) Olad, A.; Farshi Azhar, F. The Synergetic Effect of Bioactive Ceramic and Nanoclay on the Properties of Chitosan-Gelatin/Nanohydroxyapatite-Montmorillonite Scaffold for Bone Tissue Engineering. *Ceramics Intl.* **2014**, *40* (7 PART A), 10061.

(2) Thapa, K. B.; Katti, K. S.; Katti, D. R. Influence of the Fluid Polarity on Shear Strength of Sodium Montmorillonite Clay: A Steered Molecular Dynamics Study. *Comput. Geotech* **2023**, *158*, No. 105398.

(3) Echave, M. C.; Burgo, L. S.; Pedraz, J. L.; Orive, G. Gelatin as Biomaterial for Tissue Engineering. *Curr. Pharm. Des* **2017**, *23* (24), 3567.

(4) Nabavizadeh, S. S.; Shadi, M.; Khorraminejad-Shirazi, M.; Daneshi, S.; Tavanafar, S.; Naseri, R.; Abbaspour, A.; Alaei-Jahromi, K.; Talaei-Khozani, T. Moldable Alginate/Hydroxyapatite Hydrogel Loaded with Metformin Enhanced Regeneration of the Rabbit Mandibular Defects. *J. Maxillofac Oral Surg* **2024**, *23* (6), 1391.

(5) Nawang, R.; Hussein, M. Z.; Matori, K. A.; Che Abdullah, C. A.; Hashim, M. Physicochemical Properties of Hydroxyapatite/Montmorillonite Nanocomposite Prepared by Powder Sintering. *Results Phys.* **2019**, *15*, No. 102540.

(6) Ulfah, I. M.; Herdianto, N.; Aisah, N.; Fitriani, D. A.; Kurniawati, F.; Gustiono, D.; Rianti, W.; Tasomara, R.; Setiawan, J.; Ekariyani, N. Y.; Triwibowo, B.; Supriyatna, Y. I.; Ikhsan, A. N.; Masruroh, M. Effect of Porogen Agent on the Size, Shape, and Structure of Porous Hydroxyapatite Scaffolds. *Res. Biomed. Eng.* **2024**, 307.

(7) Garduño García, M. V.; Reyes Gasga, J. La Hidroxiapatita, Su Importancia En Los Tejidos Tejidos Mineralizados Y Su Aplicación Biomédica. *TIP Rev.Esp.Cienc.Quím.Biol.* 2017, *90* (2).

(8) de Pedro, J. A.; Blanco, J.; Salvado, M.; de Cabo, A.; Domínguez, J.; Cuadrado, M. A.; Pérez-Caballer, A. Inducción y Regeneración Ósea Experimental Con Proteína Morfogenética Ósea y Biomateriales. *Revista de Ortopedia y Traumatología* **2005**, *49*, 17.

(9) Kirsch, M.; Kremer, H.; Fabbri, C.; Capdevielle, P.; Collignon, F.; Mainard, D. Osseointegration of a Hydroxyapatite-Coated Stem in

Femoral Neck Fractures in the over-80 s. *European Journal of Orthopaedic Surgery and Traumatology* **2024**, *34*, 1535.
(10) Fiscal-Ladino, J. A.; Obando-Ceballos, M.; Rosero-Moreano, M.; Montaño, D. F.; Cardona, W.; Giraldo, L. F.; Richter, P. Ionic Liquids Intercalated in Montmorillonite as the Sorptive Phase for the Extraction of Low-Polarity Organic Compounds from Water by Rotating-Disk Sorptive Extraction. *Anal. Chim. Acta* **2017**, *953*, 23.
(11) Uddin, F. Montmorillonite: An Introduction to Properties and Utilization. *In Current Topics in the Utilization of Clay in Industrial and Medical Applications* **2018**.
(12) Sikdar, D.; Katti, D.; Katti, K.; Mohanty, B. Effect of Organic Modifiers on Dynamic and Static Nanomechanical Properties and Crystallinity of Intercalated Clay-Polycaprolactam Nanocomposites. *J. Appl. Polym. Sci.* **2007**, *105* (2), 790.
(13) Usuki, A.; Kawasumi, M.; Kojima, Y.; Okada, A.; Kurauchi, T.; Kamigaito, O. Swelling Behavior of Montmorillonite Cation Exchanged for ω -Amino Acids by e-Caprolactam. *J. Mater. Res.* **1993**, *8* (5), 1174.
(14) Yu, S.; Zhao, J.; Chen, G.; Juay, Y. K.; Yong, M. S. The Characteristics of Polyamide Layered-Silicate Nanocomposites. *J. Mater. Proc. Technol.* **2007**, 410−193.
(15) Zheng, J. P.; Wang, C. Z.; Wang, X. X.; Wang, H. Y.; Zhuang, H.; Yao, K. De. Preparation of Biomimetic Three-Dimensional Gelatin/Montmorillonite-Chitosan Scaffold for Tissue Engineering. *React. Funct Polym.* **2007**, *67* (9), 780.
(16) Kailasanathan, C.; Selvakumar, N. Comparative Study of Hydroxyapatite/Gelatin Composites Reinforced with Bio-Inert Ceramic Particles. *Ceram. Int.* **2012**, *38* (5), 3569.
(17) Kim, H. W.; Kim, H. E.; Salih, V. Stimulation of Osteoblast Responses to Biomimetic Nanocomposites of Gelatin-Hydroxyapatite for Tissue Engineering Scaffolds. *Biomaterials* **2005**, *26* (25), 5221.
(18) Peter, M.; Ganesh, N.; Selvamurugan, N.; Nair, S. V.; Furuike, T.; Tamura, H.; Jayakumar, R. Preparation and Characterization of Chitosan-Gelatin/Nanohydroxyapatite Composite Scaffolds for Tissue Engineering Applications. *Carbohydr. Polym.* **2010**, *80* (3), 687.
(19) Zhao, F.; Yin, Y.; Lu, W. W.; Leong, J. C.; Zhang, W.; Zhang, J.; Zhang, M.; Yao, K. Preparation and Histological Evaluation of Biomimetic Three-Dimensional Hydroxyapatite/Chitosan-Gelatin Network Composite Scaffolds. *Biomaterials* **2002**, *23* (15), 3227.
(20) Kundu, K.; Afshar, A.; Katti, D. R.; Edirisinghe, M.; Katti, K. S. Composite Nanoclay-Hydroxyapatite-Polymer Fiber Scaffolds for Bone Tissue Engineering Manufactured Using Pressurized Gyration. *Compos. Sci. Technol.* **2021**, *202*, No. 108598.
(21) Bharadwaz, A.; Jayasuriya, A. C. Recent Trends in the Application of Widely Used Natural and Synthetic Polymer Nanocomposites in Bone Tissue Regeneration. *Materials Science and Engineering C* **2020**, *110*, No. 110698.
(22) Saragih, B.; Ika Karyati, D. S. Pengaruh Pewarna Ekstrak Cair Alami Bawang Tiwai (Eleutherine Americana Merr) Terhadap Mutu Selai Kulit Pisang Kepok (Musa Paradisiaca Linn). *Jurnal Tenknologi. Pertanian* **2010**, *6* (2), 55.
(23) Narayanan, N.; Kuang, L.; Del Ponte, M.; Chain, C.; Deng, M.Design and Fabrication of Nanocomposites for Musculoskeletal Tissue Regeneration. In *Nanocomposites for Musculoskeletal Tissue Regeneration*; Woodhead Publishing 2016. .
(24) Zheng, J. P.; Li, P.; Ma, Y. L.; Yao, K. De. Gelatin/Montmorillonite Hybrid Nanocomposite. I. Preparation and Properties. *J. Appl. Polym. Sci.* **2002**, *86* (5), 1189.
(25) Zhang, Z.; Rong, Z.; Wu, G.; Wang, Y.; Tan, Z.; Zheng, J.; Jin, Y.; Liang, Z.; Liu, C.; Guo, J.; Zhu, L. Gelatin-CaO2/SAP/PLGA Composite Scaffold Enhances the Reparation of Critical-Sized Cranial Defects by Promoting Seed Cell Survival. *Appl. Mater. Today* **2021**, *22*, No. 100960.
(26) Jacobo, R.; Eugenia, M. *Análisis de La Modificación Organica de Las Arcillas Laminares (Thesis)*. 2010.
(27) Cuéllar Burgos, A.; Augusto Mesa Rueda, F.; Vargas Hernández, C.; Ernesto Perilla Perilla, J.*Arcillas modificadas caracterizadas por microraman y difraccion de rayos x modified clay characterized by microraman and xray diffraction*; Dyna 2010, *77*.
(28) Ansari, M.; Moztarzadeh, F. Effect of the Synthesis Parameters on the Properties of Biphasic Ca(OH) -HA Nanopowders for Tissue Engineering Applications. *Iran. J. Pharm. Sci.* **2012**, *8* (1), 335.
(29) Lazić, S.; Zec, S.; Miljević, N.; Milonjić, S. The Effect of Temperature on the Properties of Hydroxyapatite Precipitated from Calcium Hydroxide and Phosphoric Acid. *Thermochim. Acta* **2001**, *374* (1), 13.
(30) Imani, M. M.; Kiani, M.; Rezaei, F.; Souri, R.; Safaei, M. Optimized Synthesis of Novel Hydroxyapatite/CuO/TiO2 Nanocomposite with High Antibacterial Activity against Oral Pathogen Streptococcus Mutans. *Ceram. Int.* **2021**, *47* (23), 33398.
(31) Wei, Y.; Wang, B.; Cao, L.; Cheng, X.; Qiao, Y.; Duan, T.; He, G.; Ding, P.; Zhou, Y.; Zhou, J. Flake Channels Construction of Hydroxyapatite/Gelatin Cryogel with Excellent Flame Retardant Properties for Enhancing the Capturing of Iodine. *Collagen and leather* **2023**, *5* (1), 32.
(32) Purushotham, T.; Thangavel, A.; A.M., S.; Arumugam, P.; Raman, K. Thermal Degradation Process and Kinetics of Gelatin/HAP Composites. *ECS Trans.* **2022**, *107* (1), 16507.
(33) Deppisch, R.; Storr, M.; Buck, R.; Göhl, H. Blood Material Interactions at the Surfaces of Membranes in Medical Applications. *Sep Purif Technol.* **1998**, *14* (1−3), 241.
(34) Maina, E. W.; Wanyika, H. J.; Gacanja, A. N. Instrumental Characterization of Montmorillonite Clay by FT-IR and XRD from J.K.U.A.T Farm, in the Republic of Kenya. *Chem. Mater. Res.* **2015**, *7* (10), 43.
(35) Afraei, F.; Daneshjou, S.; Dabirmanesh, B. Synthesis and Evaluation of Nanosystem Containing Chondroitinase ABCI Based on Hydroxyapatite. *AMB Express* **2024**, *14* (1), 23.
(36) ÖNAL, M. Determination of Some Physicochemical Properties of a Hexylamine Treated Sodium Bentonite. *Communications, Faculty Of Science, University of Ankara Series B Chemistry and Chemical Engineering* **2002**, No. 001.
(37) Bertuoli, P. T.; Piazza, D.; Scienza, L. C.; Zattera, A. J. Preparation and Characterization of Montmorillonite Modified with 3-Aminopropyltriethoxysilane. *Appl. Clay Sci.* **2014**, *87*, 46.
(38) SL Shanthi, P. M.; Ashok, M.; Balasubramanian, T.; Riyasdeen, A.; Akbarsha, M. A. Synthesis and Characterization of Nano-Hydroxyapatite at Ambient Temperature Using Cationic Surfactant. *Materials Letters* **2009**, *63*, 2123−25.
(39) Popa, C. L.; Albu, M.; Bartha, C.; Costescu, A.; Luculescu, C.; Trusca, R.; Antohe, S. Structural Characterization and Optical Properties of Hydroxyapatite/Collagen Matrix. *Rom Rep. Phys.* **2016**, *68* (3), 1149.
(40) Panzavolta, S.; Fini, M.; Nicoletti, A.; Bracci, B.; Rubini, K.; Giardino, R.; Bigi, A. Porous Composite Scaffolds Based on Gelatin and Partially Hydrolyzed α-Tricalcium Phosphate. *Acta Biomater* **2009**, *5* (2), 636.
(41) Sahoo, R.; Sahoo, S.; Sahoo, S.; Nayak, P. L. Synthesis and Characterization of Polycaprolactone - Gelatin Nanocomposites for Control Release Anticancer Drug Paclitaxel. *Eur. J. Sci. Res.* 2011, *48* (3).
(42) Usuga-Manco, L. M.; López-Valdivieso, A.; Bustamante-Rúa, M. O. Estudio de La Hidrofobicidad de La Caolinita de La Unión, Antioquia. *TecnoLógicas* **2015**, *18* (35), 71.
(43) Chaibi, H.; Ftiti, Z. Credit Risk Determinants: Evidence from a Cross-Country Study. *Res. Int. Bus Finance* **2015**, *33*, 1−16.
(44) Betancur, B.; Jiménez, D.; Linares, G. Zeta Potential (ζ) as a Criterion for Optimization of Coagulant Dosage in a Drinking Water Treatment Plant. *Dyna* **2012**, *79* (175), 166.
(45) Kar, S.; Kaur, T.; Thirugnanam, A. Microwave-Assisted Synthesis of Porous Chitosan-Modified Montmorillonite-Hydroxyapatite Composite Scaffolds. *Int. J. Biol. Macromol.* **2016**, *82*, 628−636.
(46) Laabd, M.; Brahmi, Y.; El Ibrahimi, B.; Hsini, A.; Toufik, E.; Abdellaoui, Y.; Abou Oualid, H.; El Ouardi, M.; Albourine, A. A Novel Mesoporous Hydroxyapatite@Montmorillonite Hybrid Composite for High-Performance Removal of Emerging Ciprofloxacin Antibiotic from Water: Integrated Experimental and Monte Carlo Computational Assessment. *J. Mol. Liq.* **2021**, *338*, No. 116705.

https://doi.org/10.1021/acsomega.4c10725
ACS Omega 2025, 10, 15116−15128

(47) Rodrigues, S. N.; Gonçalves, I. C.; Martins, M. C. L.; Barbosa, M. A.; Ratner, B. D. Fibrinogen Adsorption, Platelet Adhesion and Activation on Mixed Hydroxyl-/Methyl-Terminated Self-Assembled Monolayers. *Biomaterials* **2006**, *27* (31), 5357.
(48) Marques, A. P.; Reis, R. L. Hydroxyapatite Reinforcement of Different Starch-Based Polymers Affects Osteoblast-like Cells Adhesion/Spreading and Proliferation. In. *Materials Science and Engineering C* **2005**, *25*, 215.
(49) Torres-Mansilla, A.; Álvarez-Lloret, P.; Voltes-Martínez, A.; López-Ruiz, E.; Baldión, P. A.; Marchal, J. A.; Gómez-Morales, J. Apatite-Coated Outer Layer Eggshell Membrane: A Novel Osteoinductive Biohybrid Composite for Guided Bone/Tissue Regeneration. *Biomaterials Advances* **2023**, *154*, No. 213605.
(50) Zhang, Y.; Luo, S.; Wang, Q.; Ramachandran, C. S. Effect of Hydrothermal Treatment on the Surface Characteristics and Bioactivity of HAP Based MAO Coating on Ti-6Al-4V Alloy. *Surf. Coat. Technol.* **2023**, *464*, No. 129566.
(51) Samadikuchaksaraei, A.; Gholipourmalekabadi, M.; Erfani Ezadyar, E.; Azami, M.; Mozafari, M.; Johari, B.; Kargozar, S.; Jameie, S. B.; Korourian, A.; Seifalian, A. M. Fabrication and in Vivo Evaluation of an Osteoblast-Conditioned Nano-Hydroxyapatite/Gelatin Composite Scaffold for Bone Tissue Regeneration. *J. Biomed Mater. Res. A* **2016**, *104* (8), 2001.
(52) Li, J.; Sun, H.; Sun, D.; Yao, Y.; Yao, F.; Yao, K. Biomimetic Multicomponent Polysaccharide/Nano-Hydroxyapatite Composites for Bone Tissue Engineering. *Carbohydr. Polym.* **2011**, *85* (4), 885.
(53) Sequeda, L. G.; Díaz, J. M.; Gutiérrez, S. J.; Perdomo, S. J.; Gómez, O. L. Obtención de Hidroxiapatita Sintética Por Tres Métodos Diferentes y Su Caracterización Para Ser Utilizada Como Sustituto Óseo. *Rev. Colomb. Cienc. Quim.-Farm.* **2012**, *41* (1), 50.
(54) Rajan, S. T.; Das, M.; Arockiarajan, A. Biocompatibility and Corrosion Evaluation of Niobium Oxide Coated AZ31B Alloy for Biodegradable Implants. *Colloids Surf. B Biointerfaces* **2022**, *212*, No. 112342.
(55) Kokubo, T.; Takadama, H. How Useful Is SBF in Predicting in Vivo Bone Bioactivity? *Biomaterials* **2006**, *27* (15), 2907.

https://doi.org/10.1021/acsomega.4c10725
ACS Omega 2025, 10, 15116−15128